Low- and High-Speed Control Strategy for PMSM Drive System Based on MMC

Jianfei ZHAO, Sucheng HUANG, and Yuanyuan XING

***Abstract*—This paper proposes a modular multilevel converter (MMC)-based control strategy for high-power permanent magnet synchronous motors (PMSM), covering both low- and high-speed ranges in electric vehicle applications. Specifically, an improved hybrid injection method based on phase voltage harmonics is introduced. The injection waveform is optimized considering the common-mode voltage, high-frequency circulating current, and phase voltage to minimize capacitor voltage fluctuations. In addition, a novel quasi-proportional-resonant (quasi-PR) controller based on an enhanced filter is developed to mitigate circulating current issues. Experimental results demonstrate that the proposed hybrid injection method effectively suppresses capacitor voltage fluctuations, reduces bridge-arm current amplitude, and improves system stability. Furthermore, the proposed quasi-PR controller achieves lower circulating current and further enhances system robustness and disturbance rejection capability.**

***Index Terms*—Circulating current suppression, modular multilevel converter, permanent magnet synchronous motor, suppression of capacitor voltage fluctuations.**

I. Introduction

In light of the accelerated growth of the new energy sector, there has been a notable increase in research activity within the field of motor drive systems. The utilization of medium-voltage and high-voltage converters for the speed control of high-power permanent magnet synchronous motor (PMSM) has the potential to significantly reduce energy consumption, enhance the speed control performance and extend the operational lifespan of the motor [1]. The modular multilevel converter (MMC) exhibits advantageous characteristics, including high reliability, high-power quality and high-voltage level [2]. These attributes position the MMC as a promising candidate for advancement in the domain of high-power motor drive systems [3].

MMC application to PMSM control is associated with significant capacitor voltage fluctuations during motor startup and low-speed operation. This fluctuation results from low load current, which causes current imbalance across submodules and inefficient capacitor charging. The high switching frequency of the MMC converter can further exacerbate the issue by introducing ripple currents, increasing voltage variations. Minimizing these fluctuations is crucial for stable PMSM operation, especially at low speeds. Excessive capacitor voltage fluctuations can cause submodule overvoltage, waveform distortion, and system instability [4]. In 2010, ABB proposed a method [5] and enabled the startup of the induction motor [6], which involved injecting high-frequency common-mode voltage at the AC output side and high-frequency current into the three-phase circulating current. [7] proposed an adaptive switching frequency control method for carrier phase-shift modulation, which improves the system's efficiency by dynamically adjusting the switching frequency. This method enhances the modulation strategy in the MMC, contributing to more stable operation and reduced voltage fluctuation. The high-frequency injection method generates common-mode voltage by injecting high-frequency current through the ground capacitor, causing interference between the ground and signal lines. This increases bearing wear but effectively reduces capacitor voltage fluctuations at low-speed PMSM operation by balancing the current across MMC submodules and improving energy distribution [8]. [9] proposed a flying-capacitor MMC (FCMMC) to attain power balance between the upper and lower bridge-arms without the injection of a common-mode voltage. The concept of the star and delta channel MMC was first proposed in [10] and [11] respectively. In essence, the full bridge sub-modules were connected to the midpoint of the three-phase bridge-arms using star/delta connections, injecting high-frequency circulating current by generating a regulation voltage. In addition to introducing common-mode interference, the high-frequency circulating current injected by the high-frequency injection also resulted in elevated bridge-arm currents [12]. The injected common-mode voltage waveform was modified from a sine wave to a square-wave, thereby reducing the requisite injected current amplitude [13]. [14] employed a delay treatment at the square-wave mutation and replaced the square-wave with trapezoidal waveform.

Consequently, the low frequency suppression scheme based on the high-frequency injection method is more widely applicable. However, for constant torque loads, further reducing the amplitude of high-frequency circulating currents

Manuscript received May 8, 2025; revised July 14, 2025; accepted August 15, 2025. Date of publication December 30, 2025; date of current version September 9, 2025. No funding was received to assist with the preparation of this manuscript. *(Corresponding author: Jianfei Zhao.)*

All authors are with School of Mechatronic Engineering and Automation, Shanghai University, Shanghai 200444, China (e-mail: jfzhao@shu.edu.cn; Mr_huang@shu.edu.cn; xingyuanyuan@shu.edu.cn).

Digital Object Identifier 10.24295/CPSSTPEA.2025.00030

while suppressing capacitor voltage fluctuations remains an area for further study.

As the motor speed increases, the capacitor voltage fluctuation decreases. However, it leads to an increase in circulating current, which becomes a more significant issue. Harmonic components in circulating currents cause distortion of bridge-arm currents, increasing current demand and switching losses [15]. A novel proportional integral and resonance control was devised to achieve the static free tracking of the fundamental frequency components and the control of the high-frequency harmonic components [16]. [17] integrated fuzzy control with traditional PI control, proposing a method based on fuzzy adaptive PI control. Furthermore, circulation suppression could be achieved by improving the network topology, adjusting the modulation strategy, and modelling the network state. [18] replaced the half bridge submodule with full bridge submodule, allowing the MMC to operate at full power without overmodulation. [19] suggested a method based on the use of dead band control mechanism.

A number of other scholars have concentrated their efforts on providing theoretical guidance for the design and optimization of MMC circulation suppression methods. [20] presented a method to calculate the circulating current in a synchronous rotating coordinate system. [21] proposed an MMC small signal modelling method based on harmonic state space equations. In [22], a novel DC impedance model was put forth to address the deficiencies of the extant MMC DC impedance model, which failed to incorporate the internal dynamic performance of the MMC. [23] put forth an optimal second harmonic component injection strategy while ignoring the potential loss imbalance between the submodule power devices. However, most of the aforementioned methods neglected the existence of higher-frequency components in the circulating current such as the quadruple frequency circulating component [24]. Therefore, there has been significant essential to investigate strategies for suppressing circulating currents to develop more effective suppression methods.

This paper can be summarized as follows: Section II analyses MMC working principle and proposes the improved hybrid injection method based on phase voltage harmonic. Section III presents a novel quasi-PR control circulating current suppression strategy based on enhanced adaptive filter. Section IV evaluates the simulation results. Section V builds an experimental platform to verify the effectiveness of the proposed control strategy. Finally, the conclusion and references are presented.

II. Improved Hybrid Injection Low Frequency Suppression Method Based on Phase Voltage Harmonic

A. MMC Working Principle

Fig. 1 shows the MMC PMSM circuit topology.

The MMC circuit consists of three-phase units, each comprising N submodules and a bridge-arm inductance L_{arm}. where U_{dc} is the DC side voltage; I_{dc} is the DC side current;

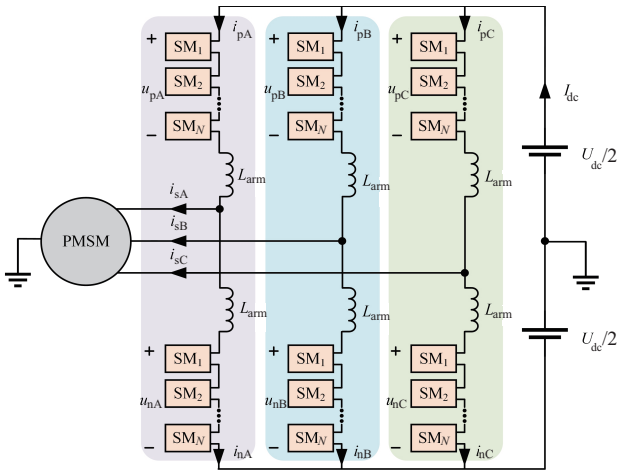

Fig. 1. MMC and PMSM circuit topology structure

u_{pj} and u_{nj} are the upper and lower bridge-arm voltages; i_{pj} and i_{nj} are the upper and lower bridge-arm currents; i_{sj} is the three-phase current.

Suppose the phase voltage can be expressed as:

$$u_{sj} = U_{sm}\sin(\omega t) = m\frac{U_{dc}}{2}\sin(\omega t) \tag{1}$$

where U_{sm} is the amplitude of the phase voltage; ω is the angular frequency; m is the voltage modulation ratio; and the specific expression is:

$$m = \frac{U_{sm}}{U_{dc}/2} \tag{2}$$

Assume that the phase current can be expressed as:

$$i_{sj} = I_{sm}\sin(\omega t + \varphi) \tag{3}$$

where I_{sm} is the amplitude of the phase current and φ is the power factor angle of the AC side.

There is current flowing directly through the upper and lower bridge-arms during the operation of the MMC. The non-fundamental frequency component of this current is generally referred to as the circulating current i_{cirj}. According to Kirchhoff's current law, the j-phase upper and lower bridge-arm currents can be expressed as:

$$i_{pj} = i_{cirj} + \frac{i_{sj}}{2} \tag{4}$$

$$i_{nj} = i_{cirj} - \frac{i_{sj}}{2} \tag{5}$$

where i_{pj} is upper bridge-arm current; i_{nj} is the lower bridge-arm current.

B. Dual-Sinusoidal Injection Method

In the double-sine injection method, the injected high-

frequency common-mode voltage u_{cm} and high-frequency circulating current i_{cm} are written as:

$$u_{cm} = U_{cm}\sin(\omega_h t) \tag{6}$$

$$i_{cm} = I_{cm}\sin(\omega_h t) \tag{7}$$

where U_{cm} and I_{cm} are the amplitude of high-frequency common-mode voltage and circulating current separately; ω_h is common-mode voltage angular frequency $\omega_h = 2\pi f_h$; f_h is common-mode voltage frequency.

The fundamental frequency component in bridge-arm power p_{low} can be expressed as:

$$p_{low} = \frac{U_{dc} i_{sj}}{4}[1 - m^2\sin^2(\omega t + \eta_{sj})] \tag{8}$$

The amplitude of high-frequency circulating current needed to be injected is:

$$I_{cm} = \frac{U_{dc} i_{sj}}{2U_{cm}}[1 - m^2\sin^2(\omega t)] \tag{9}$$

From (9), U_{cm} is in inverse proportion to I_{cm}. Since U_{cm} is limited by the duty cycle and U_{dc}, U_{cm} must meet the following requirements to prevent overmodulation:

$$U_{cm} \leqslant \frac{(1-m)}{K}\frac{U_{dc}}{2} \tag{10}$$

The range of K in (10) is 1−1.2. According to (9), when U_{cm} takes the maximum value, I_{cm} can be given by:

$$I_{cm} = \frac{K i_{sj}}{1-m}[1 - m^2\sin^2(\omega t + \eta_{sj})] \tag{11}$$

C. Design of Improved Hybrid Injection Method Based on Phase Voltage Harmonics

High-frequency square-wave common-mode voltage and circulating current injection can improve waveform utilization. However, the presence of abundant harmonics necessitates tracking both the fundamental frequency ω_h and its third harmonic $3\omega_h$, thereby imposing stricter requirements on the control bandwidth compared to the dual-sinusoidal injection method. Moreover, when the square-wave circulating current passes through the bridge-arm inductance, it may cause a steep voltage spike at the current's zero-crossing point.

To address these issues, square-wave injection is replaced by a combined sinusoidal and third harmonic waveform. To address these issues, square-wave injection is replaced by a combined sinusoidal and third harmonic waveform. This composite waveform not only approximates the square wave to retain its high fundamental voltage utilization but also smooths the current waveform, thereby reducing voltage spikes across the bridge-arm inductance. The third harmonic component adjusts the waveform shape to suppress abrupt transitions near zero crossings, improving modulation stability and lowering the amplitude of the required circulating current. This reduces switching stress and enhances converter efficiency under low-speed conditions.

TABLE I
INTERVAL SELECTION

u_{sA}	u_{sB}	u_{sC}	Interval
+	+	−	1
−	+	−	2
−	+	+	3
−	−	+	4
+	−	+	5
+	−	−	6

The injected common-mode voltage u_{cm} and circulating current i_{cm} are given by:

$$u_{cm} = \begin{cases} -U_{cm} & (0 < t \leqslant \dfrac{1}{2f_h}) \\ U_{cm} & (\dfrac{1}{2f_h} < t < \dfrac{1}{f_h}) \end{cases} \tag{12}$$

$$i_{cm} = I_{cm}[\sin(\omega_h t) + \frac{1}{6}\sin(3\omega_h t)] \tag{13}$$

In order to increase the speed of command input and to reduce the calculation session time, the look-up table method is used for phase voltage harmonic injection. The process is: Firstly, three-phase sinusoidal voltage u_{sA}, u_{sB}, and u_{sC} were obtained by vector control. Then, select the corresponding intervals according to positive and negative three-phase voltage values and Table I. Finally, compare the magnitude of the same positive and negative sign voltages to get the injected voltage u_z. Table I is the interval selection table.

Interval 1:
If $|u_{sA}| \geqslant |u_{sB}|$, $u_z = u_{sB}/2$; If $|u_{sA}| < |u_{sB}|$, $u_z = u_{sA}/2$.
Interval 2:
If $|u_{sA}| \geqslant |u_{sC}|$, $u_z = u_{sC}/2$; If $|u_{sA}| < |u_{sC}|$, $u_z = u_{sA}/2$.
Interval 3:
If $|u_{sB}| \geqslant |u_{sC}|$, $u_z = u_{sC}/2$; If $|u_{sB}| < |u_{sC}|$, $u_z = u_{sB}/2$.
Interval 4:
If $|u_{sB}| \geqslant |u_{sA}|$, $u_z = u_{sA}/2$; If $|u_{sB}| < |u_{sA}|$, $u_z = u_{sB}/2$.
Interval 5:
If $|u_{sC}| \geqslant |u_{sA}|$, $u_z = u_{sA}/2$; If $|u_{sC}| < |u_{sA}|$, $u_z = u_{sC}/2$.
Interval 6:
If $|u_{sC}| \geqslant |u_{sB}|$, $u_z = u_{sB}/2$; If $|u_{sC}| < |u_{sB}|$, $u_z = u_{sC}/2$.

The three-phase voltage after harmonic injection u'_{sj} can be written as:

$$u'_{sj} = u_{sj} + u_z \tag{14}$$

After harmonic injection, the amplitude of the phase voltage

is 0.87 times the amplitude of its fundamental component. The fundamental utilization is higher than that of sine wave of the same amplitude. Thus, the range of values for U_{cm} is further increased:

$$U_{cm} \leqslant \frac{(1-0.87m)}{K}\frac{U_{dc}}{2} \tag{15}$$

After third harmonic injection, the low frequency component of the bridge-arm power p'_{low} can be expressed as:

$$p'_{low} = \frac{U_{dc} i_{sj}}{4}[1 - m^2 \sin^2(\omega t + \eta_{sj}) - \frac{m^2}{24}\sin^2(\omega t + \eta_{sj})] \tag{16}$$

In addition, the amplitude of the injected high-frequency circulating current I_{cm} is written as:

$$I_{cm} = \frac{36\pi}{304}\frac{U_{dc} i_{sj}}{U_{cm}}[1 - m^2 \sin^2(\omega t + \eta_{sj}) - \frac{m^2}{24}\sin^2(\omega t + \eta_{sj})] \tag{17}$$

Take the maximum of U_{cm} in (15) and substitute it into (17). Then, the required injection circulating current amplitude in the phase voltage harmonic improvement hybrid injection method can be expressed as:

$$I_{cm} = \frac{72\pi}{304}\frac{K i_{sj}}{1-0.87m}[1 - m^2 \sin^2(\omega t + \eta_{sj}) - \frac{m^2}{24}\sin^2(\omega t + \eta_{sj})] \tag{18}$$

Capacitor voltage fluctuation decreases as motor speed increases. Thus, the fluctuation will be acceptable for normal operation after the motor speed reaches a certain value. The injection control strategy proposed in this chapter is only applicable to the low speed condition of the motor. And different system parameters have different speed cut-off points. In this paper, the MMC is selected to start up with 0.5 N·m light load. The calculation shows that when the rotational speed is 200 rpm, the fluctuation range has been reduced to 20% of the rated capacitor voltage. Therefore, in this paper, the speed is divided into a low speed band of 0−200 rpm and a medium-high speed band of 200−900 rpm.

In summary, the control diagram of the low frequency suppression strategy proposed in this paper is shown in Fig. 2.

The system control structure consists of: 1) A classic speed-current double closed-loop control. 2) Given high-frequency circulating current tracking, i_{cm} is obtained according to (18) and u_{cj} is obtained through the P controller. 3) High-frequency common-mode voltage injection. u_{cm} is accessed by (12). 4) Phase voltage harmonics injection. u'_{sj} is acquired by (14).

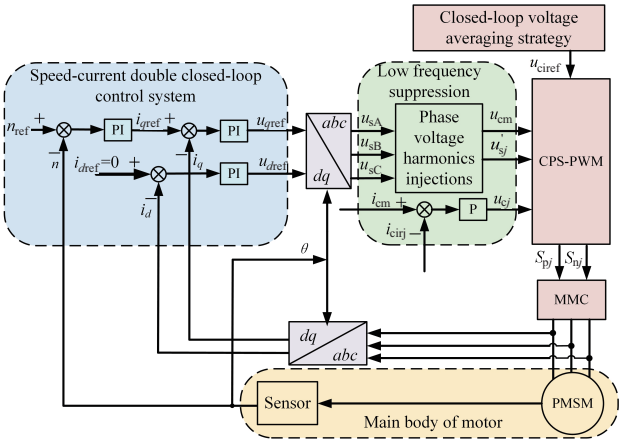

Fig. 2. The control diagram of the low-frequency suppression strategy proposed in this paper.

5) Closed loop voltage averaging strategy. The u_{ciref} of each submodule is obtained through the P controller. 6) Carrier phase shifted pulse width modulation (CPS-PWM). The switching function for the MMC part is obtained.

III. A Novel Quasi-PR Control Circulating Current Suppression Strategy Based on Enhanced Adaptive Filters

A. MMC Circulating Current Analysis

The expression for circulating current is:

$$\begin{cases} i_{cira} = \dfrac{I_{dc}}{3} + \sum_{n=2}^{\infty} nI_{nm}\cos(n\omega_n t + \theta_{nm}) \\ i_{cirb} = \dfrac{I_{dc}}{3} + \sum_{n=2}^{\infty} nI_{nm}\cos\left[n(\omega_n t - \dfrac{2\pi}{3}) + \theta_{nm}\right] \\ i_{cirb} = \dfrac{I_{dc}}{3} + \sum_{n=2}^{\infty} nI_{nm}\cos\left[n(\omega_n t + \dfrac{2\pi}{3}) + \theta_{nm}\right] \end{cases} \tag{19}$$

where I_{nm} and θ_{nm} are separately the peak and the initial phase of circulating current harmonics after n times; and i_{cira}, i_{cirb}, i_{circ} are circulating current in three-phase circuits.

From (19), the circulating current actually consists of a DC component $I_{dc}/3$ and even harmonics such as second, fourth, and sixth component. The amplitude is inversely proportional to the frequency. The circulating current is specified as a voltage drop across the bridge-arm inductance. Therefore, the circulating current can be suppressed by superimposing a suppression component of the same phase sequence on the voltage modulating waveform of the upper and lower bridge-arms, thereby generating a reverse inductive voltage drop u_{csj}.

Since the circulating current harmonics are dominated by the second frequency component, based on the principle of vector control, the negative sequence second frequency rotating coordinate system can be used to transform the second frequency circulating current into a direct current and then suppress it by using a PI controller. Fig. 3 shows the MMC

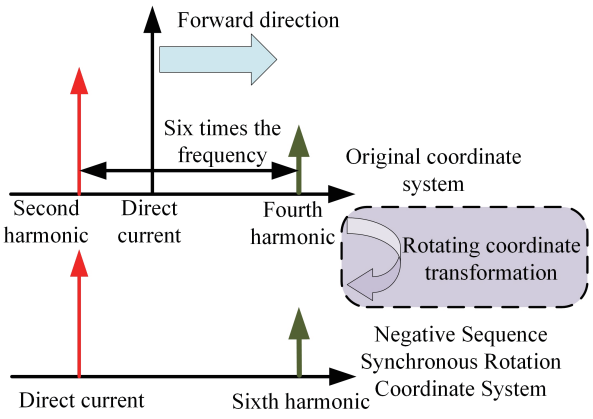

Fig. 3. MMC circulation spectrum diagram.

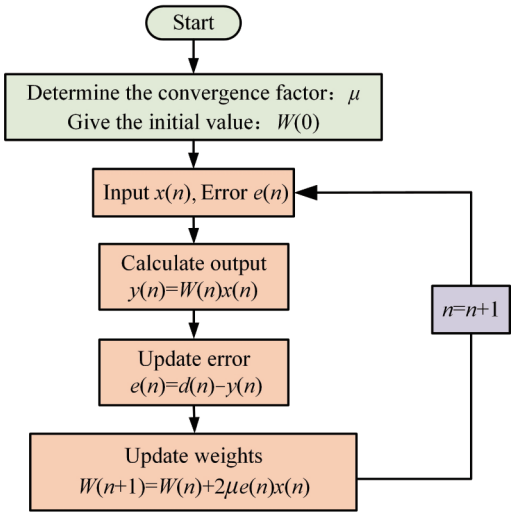

Fig. 4. LMS adaptive algorithm flowchart.

circulating current spectrum, where the horizontal coordinate is the direction and the vertical coordinate is the amplitude.

However, due to the presence of other harmonics in the circulating current, the component obtained after the coordinate transformation is not a complete direct current.

As shown in Fig. 3, the left side of the horizontal axis represents the second harmonic component and the right is the fourth harmonic, and the distance between them is the sixth harmonic. The fourth circulating current harmonic becomes the sixth harmonic in the negative sequence synchronous rotating coordinate system, and the presence of the sixth harmonic leads to poor tracking and suppression of the circulating current by the PI controller.

B. Design of Improved Adaptive Filter

The least mean squares (LMS) algorithm is an important method in adaptive filter design, which has the advantages of simple principle, few parameters, easy to implement and small computation, etc. The algorithm flowchart is shown in Fig. 4.

The adaptive filter should converge faster and exhibit smaller steady-state error under external disturbances. A fixed convergence coefficient involves a trade-off between speed and stability, whereas a time-varying coefficient can dynamically balance both through iterative adaptation. The new weight coefficient update formula is:

$$W(n+1)=W(n)+2\mu(n)e(n)x(n) \tag{20}$$

The criterion for the variable step-size LMS algorithm is as follows: a larger step size is used in the early stage of iteration to achieve fast convergence, while a smaller step size is used in the later stage to improve steady state performance when the system reaches steady state. To overcome the convergence-stability trade-off in conventional LMS filters, we introduce a variable-step strategy using a sigmoid function. The function dynamically increases the convergence rate during large-error conditions and decreases it as the error reduces, improving both response speed and steady-state accuracy. This approach is novel in the context of harmonic suppression for MMC-driven PMSM systems.

The function is transformed based on the sigmoid function to better match the function curve to the convergence coefficient adjustment criterion. In addition, a compensation factor is introduced to improve the characteristics at the lower end of the function by dynamically adjusting the convergence coefficient of the algorithm. The resulting updating formula is:

$$\mu(n)=a\left[1-\frac{1+b}{1+b(\exp(c\left|e(n)e(n-1)\right|)+k\left|e(n-1)\right|)}\right] \tag{21}$$

where k is the compensation coefficient, which is assumed to be 0.01; a, b, and c are the adjustment coefficients:

1) The parameter a can set an upper bound for the convergence coefficient so the value of μ ranges from (0, a].

2) The parameter b primarily affects the lower end characteristics of the convergence coefficient variation curve.

3) The parameter c primarily influences the variation amplitude of the convergence coefficient as $e(n)$ approaches 0.

C. Design of Circulating Current Suppressor Based on Quasi-PR Control

The harmonics of the MMC circulating current are mainly composed of the direct flow and the second component, so the expression of the circulating current is given by:

$$i_{\text{cir}j}=\frac{I_{\text{dc}}}{3}+w_{2f\_1}\cos(2\theta)+w_{2f\_2}\sin(2\theta) \tag{22}$$

Adaptive filters use error feedback from an adaptive algorithm to adjust the convergence and weighting coefficients to better track harmonic currents. The adaptive filter output is the circulating current harmonics:

$$y(n)=w_1\cos(2\theta)+w_2\sin(2\theta)=w_1x_1(n)+w_2x_2(n) \tag{23}$$

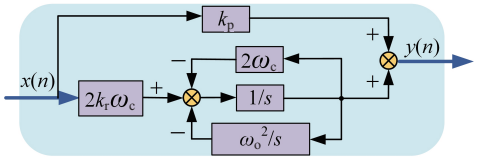

Fig. 5. Structure of quasi-PR controller.

The error is calculated as:

$$e(n) = i_{cirj} - y(n) \tag{24}$$

The LMS algorithm update formula is:

$$\begin{cases} w_1(n+1) = w_1(n) + 2\mu(n)e(n)x_1(n) \\ w_2(n+1) = w_2(n) + 2\mu(n)e(n)x_2(n) \end{cases} \tag{25}$$

The quasi-PR controller introduces a resonant peak at a target frequency in the stationary $\alpha\beta$ frame. It eliminates the need for coordinate transformation while providing strong harmonic suppression for fixed-frequency circulating current components. This approach simplifies implementation, avoids frequency mismatch, and is novel in MMC-PMSM systems when used in conjunction with hybrid injection. The specific structure is shown in Fig. 5. Its transfer function is:

$$G_{QPR}(s) = k_p + \frac{2k_r\omega_c s}{s^2 + 2\omega_c s + \omega_o^2} \tag{26}$$

where k_p and k_r are the proportional gain and resonant gain; ω_o is the resonant frequency and ω_c is the cut-off frequency.

The PR controller uses predistorted bilinear transformation:

$$s = \frac{\omega_o}{\tan(0.5\omega_o T_s)} \frac{1 - z^{-1}}{1 + z^{-1}} \tag{27}$$

Combining the z inverse transformation:

$$\begin{aligned} y(k) = k_r[&\frac{b_1}{2\omega_o a_1} e(k) + \frac{b_2}{2\omega_o a_1} e(k-2)] - \\ &\frac{a_2}{a_1} y(k-1) - \frac{a_3}{a_2} y(k-2) \end{aligned} \tag{28}$$

where the parameters are:

$$\begin{cases} a_1 = 1 + \dfrac{\omega_c}{\omega_o}\sin(\omega_o T_s) \\ a_2 = -2\cos(\omega_o T_s) \\ a_3 = 1 - \dfrac{\omega_c}{\omega_o}\sin(\omega_o T_s) \\ b_1 = -b_2 = \omega_c \sin(\omega_o T_s) \end{cases} \tag{29}$$

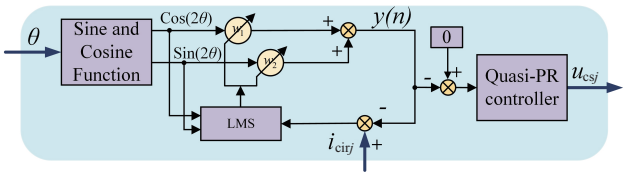

Fig. 6. Novel type of circulating current suppressor.

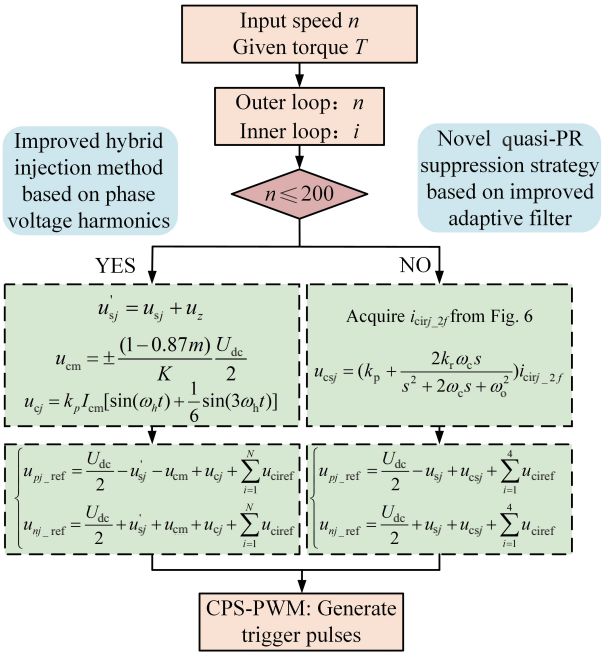

Fig. 7. Overall block diagram of high and low speed control.

The control block diagram of the novel circulating current suppressor based on the improved adaptive filter algorithm and the quasi-PR control is finally obtained as shown in Fig. 6.

The process of control action can be divided into the following three main parts:

1) First, the filter input signal is obtained using the sine-cosine function with i_{cirj} and θ as input parameters;

2) Then, the online adjustment of the circulating current harmonic amplitude weight coefficients is achieved by the variable convergence coefficient LMS algorithm;

3) Finally, with the target of turning the circulating current decreasing to 0, the u_{csj} is obtained by the quasi-PR controller and superimposed on the voltage modulated waveform of the upper and lower bridge-arms.

The overall block diagram of the MMC PMSM low- and high-speed control proposed in this paper is shown in Fig. 7.

IV. Simulation Results

Analysis of Improved hybrid injection method based on phase voltage harmonics

The three-phase five-level MMC PMSM simulation model is built according to the parameters as shown in Table II.

Under a 0.5 N·m load, the motor accelerates from 0 to 150 rpm with a frequency of 10 Hz during steady-state operation,

TABLE II
MMC PMSM SIMULATION PARAMETERS

Parameters	Value
DC bus voltage(V)	200
Number of submodules per	4
Number of motor pole pairs	4
Submodule capacitor(mF)	2.2
Bridge-arm inductor(mH)	7
System control frequency(Hz)	10000
Carrier frequency(Hz)	2000
Stator resistor(mΩ)	8
d-axis inductor(μH)	50
q-axis inductor(μH)	86

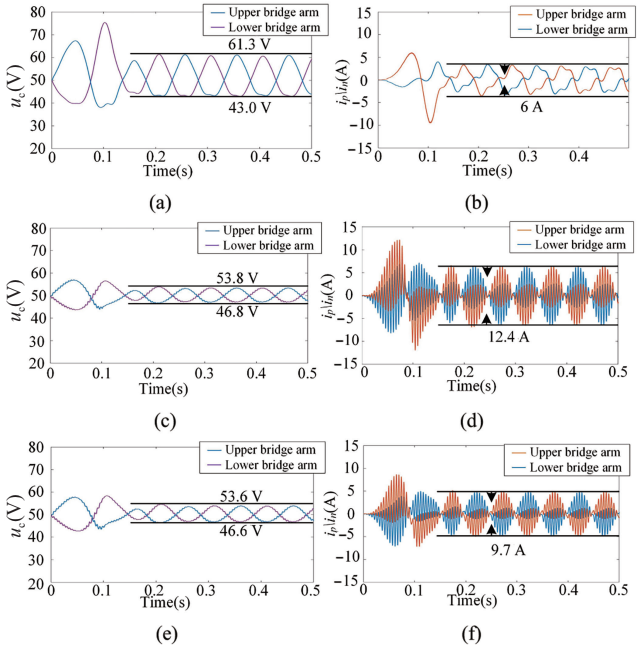

Fig. 8. (a) Capacitor voltage waveform with no high-frequency injection, (b) Bridge-arm current waveform with no high-frequency injection, (c) Capacitor voltage waveform with dual-sinusoial injection, (d) Bridge-arm current waveform with dual-sinusoial injection, (e) Capacitor voltage waveform with improved hybrid injection, (f) Bridge-arm current waveform with improved hybrid injection.

and the capacitor voltage waveform for this condition are shown in Fig. 8 shows the capacitor voltage waveform and bridge-arm current waveform under different methods.

As shown in Figs. 8(a), (c), and (e), without low-frequency suppression, the capacitor voltage fluctuates between 43 V and 61.3 V. After applying the dual-sinusoidal injection method, the fluctuation range is reduced to 46.8–53.8 V, indicating a peak-to-peak reduction of 11.3 V. The improved hybrid injection method, which incorporates phase voltage harmonic injection, achieves a similar level of fluctuation control, with a voltage range of 46.6–53.6 V.

As shown in Figs. 8(b), (d), and (f), applying the dual-sinusoidal injection method increases the peak-to-peak value of the steady-state bridge-arm current from 6 A to 12.4 A compared to the case without low-frequency suppression—an increase of 106.67%. In contrast, the proposed hybrid injection method incorporating phase voltage harmonic injection reduces the current amplitude to 9.7 A, representing a 21.17% reduction. The specific comparison results are summarized in Table III.

TABLE III
SPECIFIC DETAILS OF DIFFERENT STRATEGY

Strategy	Capacitor Voltage Fluctuation (V)	Bridge-Arm Current Peak(A)
No high-frequency injection	18.3	6
Dual-sinusoidal injection	7.0	12.4
Improved hybrid injection	7.0	9.7

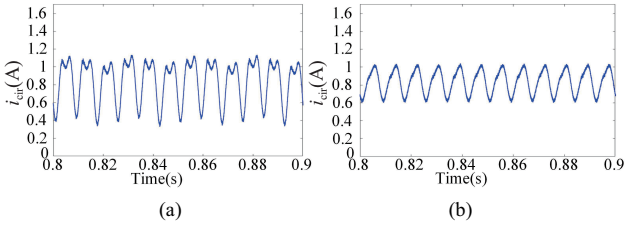

Fig. 9. Circulating current waveform. (a) CCSC, (b) Novel circulating current suppression method proposed in this paper.

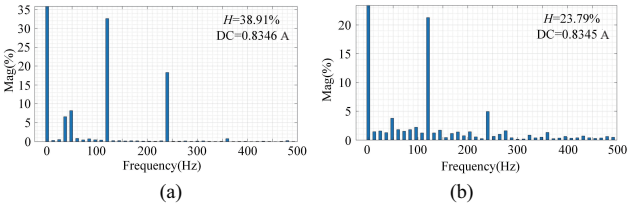

Fig. 10. FFT analysis of circulation. (a) CCSC, (b) Novel circulating current suppression method proposed in this paper.

B. Analysis of A Novel Circulating Current Suppression Method Based on Quasi-PR Control and Adaptive Filters

The harmonic inclusion rate H of the circulating current is defined to further analyse the harmonic situation:

$$H = \sqrt{I_1^2 + I_2^2 + I_3^2 \cdots + I_{\max}^2} \,/\, I \times 100\% \tag{30}$$

where I_x is the RMS value of the harmonic component of the circulating current with frequency x Hz, and I is the magnitude of the DC component of the circulating current.

The circulating current waveform of the negative sequence coordinate transform based circulating current suppression control algorithm (CCSC) and suppression algorithm proposed in this paper are shown in Fig. 9. The circulating current FFT results under the two algorithms are shown in Fig. 10.

Fig. 9 illustrates that, compared with CCSC, the proposed circulating current suppression algorithm achieves an 11.3% reduction in the second harmonic component of the circulating current. Fig. 10 demonstrates that the harmonic content of the circulating current decreases from 38.91% to 23.79%, corresponding to a 15.12% reduction.

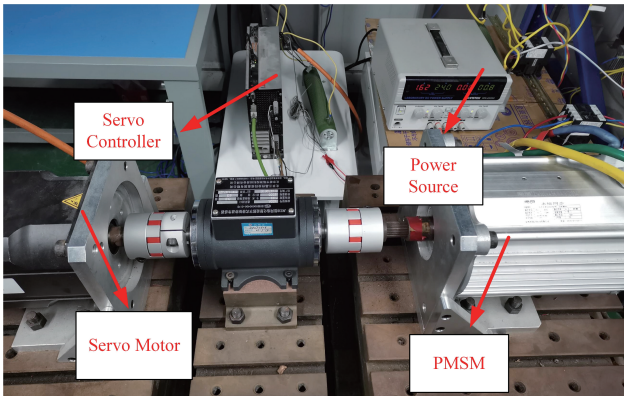

Fig. 11. Physical image of the towing motor platform.

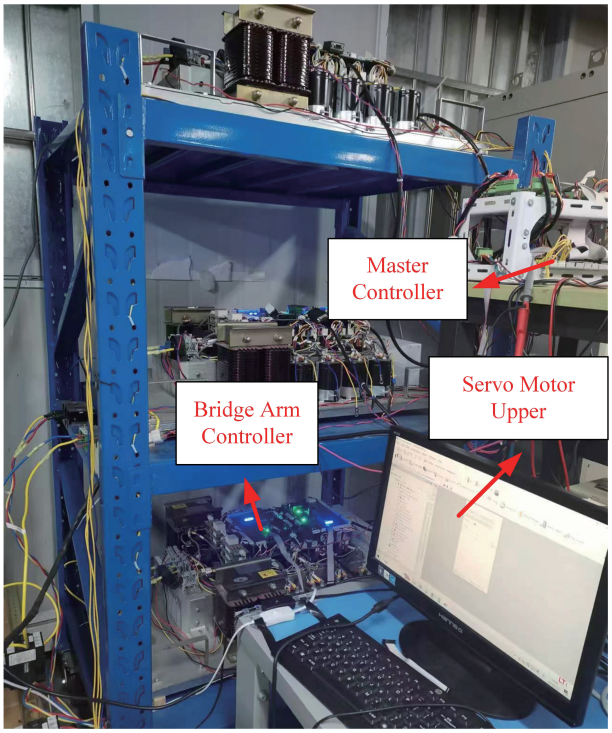

Fig. 12. MMC physical image.

V. Experimental Validation

In order to further verify the effectiveness of the proposed low-frequency suppression strategy, an experimental study was carried out on the constructed MMC PMSM experimental prototype, using the motor-to-drag platform physically shown in Fig. 11. The PMSM is connected to the MMC as the drive motor, and receives torque and speed commands from the host computer through the serial port. The servo motor and the drive motor are connected in coaxial for simulating the load.

The physical structure of the MMC prototype is shown in Fig. 12. The DC bus voltage is supplied by an external DC power source. The main circuit consists primarily of submodules installed on the six bridge arms of the three-phase system, along with the bridge-arm inductance. Each submodule adopts a half-bridge topology, and the specific device parameters are listed in Table II.

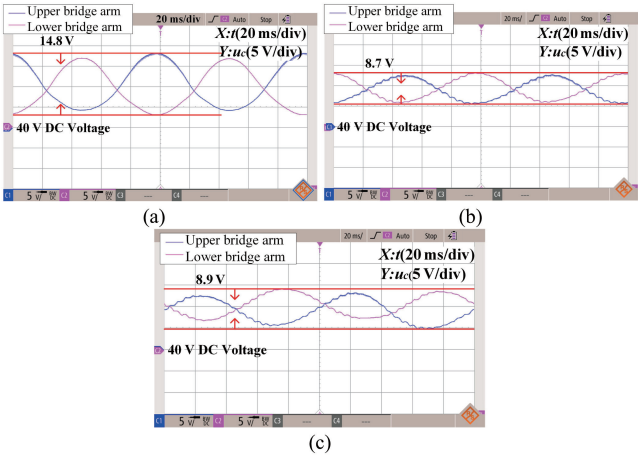

Fig. 13. Capacitor voltage waveform. (a) No high-frequency injection, (b) Dual-sinusoidal injection, (c) Improved hybrid injection based on phase voltage harmonic.

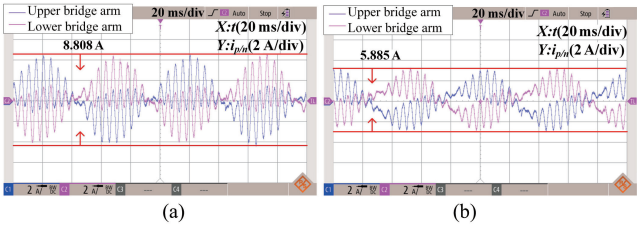

Fig. 14. Circulating current waveform. (a) Dual-sinusoidal injection, (b) Improved hybrid injection based on phase voltage harmonic.

A. Improved Hybrid Injection Method Based on Phase Voltage Harmonics

Fig. 13 shows the upper and lower bridge-arm capacitor voltage waveform under the motor speed of 150 rpm and current amplitude of 3 A.

Without low-frequency suppression, the peak capacitor voltage fluctuation reaches 14.8 V, accounting for 29.6% of the rated capacitor voltage. With the dual-sinusoidal injection method, the peak fluctuation is reduced to 8.7 V (17.4% of rated voltage), corresponding to a 12.2% suppression compared to the unsuppressed case. The proposed hybrid injection method incorporating phase voltage harmonics achieves a similar suppression effect, with a peak fluctuation of 8.9 V. The corresponding bridge-arm current waveforms under both injection methods are shown in Fig. 14.

When dual-sinusoidal injection is performed, the peak value of bridge-arm current reaches 8.808 A. When the improved hybrid injection based on phase voltage harmonic is performed, the peak value of bridge-arm current is reduced to 5.885 A, which is 33.18% lower compared to dual-sinusoidal injection method. The results indicate that the proposed hybrid injection method significantly reduces the amplitude of the injected circulating current.

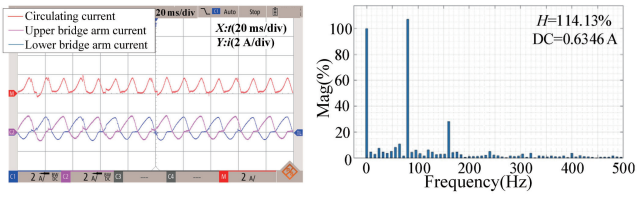

Fig. 15. No circulating current suppression. (a) B phase circulating current, (b) Circulating current FFT analysis.

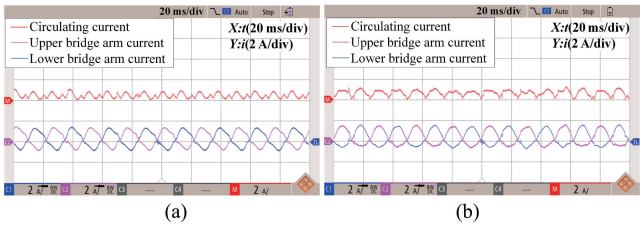

Fig. 16. B phase circulating current waveform. (a) CCSC, (b) Novel circulating current suppression.

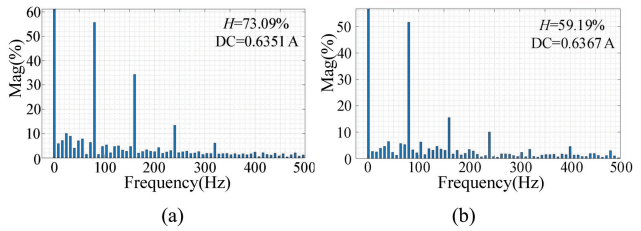

Fig. 17. Circulating current FFT analysis. (a) CCSC, (b) Novel circulating current suppression.

B. Novel Circulating Current Suppression Method Based on Quasi-PR Control and Adaptive Filter

In order to verify the effectiveness of the novel circulating current suppression method based on quasi-PR control and adaptive filter, an experimental study was carried out on the experimental prototype.

In the case of no circulating current suppression control, the motor speed is set to 600 rpm and the current amplitude is 2 A. The waveform of the B-phase upper and lower bridge-arm currents and circulating current are shown in Fig. 15(a), which corresponds to the circulating fundamental frequency of 40 Hz. The results of the circulating current FFT analysis are shown in Fig. 15(b), which shows that circulating current harmonics are mainly composed of even components such as second harmonic and fourth harmonic.

Subsequently, the CCSC and the novel circulating current suppression method based on quasi-PR control and adaptive filter were applied to the above systems. Fig. 16 illustrates the B phase circulating current waveform. Fig. 17 demonstrates the corresponding FFT analysis of this phase circulating current.

As shown in Figs. 16 and 17, the CCSC strategy reduces the harmonic containment rate H from 114.13% to 73.09%, representing a 41.04% decrease compared to the case without circulating current suppression. Additionally, the proportion of the second harmonic component relative to the DC component of the circulating current is reduced by 51.47%. Furthermore, compared to the CCSC strategy, the proposed suppression method reduces the harmonic containment rate from 73.09% to 59.19%, corresponding to a 13.90% reduction. Similarly, the proportion of the second harmonic component in the circulating current is further decreased by 4.05%. These results show that the proposed method reduces total harmonic distortion without increasing low-frequency or fourth harmonic components. This contributes to more effective circulating current suppression and enhanced efficiency of the drive system. The specific comparison results are summarized in Table IV.

TABLE IV
SPECIFIC DETAILS OF DIFFERENT STRATEGY

Strategy	Harmonic containment rate H
No circulating current suppression	114.13%
Traditional circulating current suppression (CCSC)	73.09%
Novel circulating current suppression	59.19%

VI. CONCLUSION

This paper investigates the application of MMC as a converter in electric vehicles and proposes a low-speed and high-speed control strategy for the PMSM drive system. To address the increased bridge-arm current caused by high-frequency current injection under low-speed conditions, which leads to elevated current stress on the switching devices, an improved hybrid injection strategy based on phase voltage harmonics is proposed. Furthermore, to overcome the limitations of coordinate transformation in accurately extracting the second harmonic component of the circulating current, a novel quasi-PR suppression strategy incorporating an adaptive filter is developed. Simulation and experimental results indicate that, while achieving a comparable level of capacitor voltage fluctuation suppression, the proposed method reduces the bridge-arm current by 33.19% compared with the dual-sinusoidal injection method, thereby effectively alleviating current stress on the switching devices. Compared to the conventional CCSC strategy, the proposed suppression method reduces the proportion of the second harmonic component in the circulating current by 4.05% and lowers the total circulating current harmonic content H by 13.9%, resulting in improved circulating current suppression.

Overall, the proposed strategies enhance the operational performance and robustness of electric vehicle drive systems.

REFERENCES

[1] A. Viatkin, M. Ricco, R. Mandrioli, T. Kerekes, R. Teodorescu, and G. Grandi, "A novel modular multilevel converter based on interleaved half-bridge submodules," in *IEEE Transactions on Industrial Electronics*, vol. 70, no. 1, pp. 125–136, Jan. 2023.

[2] Y. Zhang, S. Li, X. Zhang, C. Liu, Z. Liu, and B. Luo, "A hybrid low

capacitance modular multilevel converter for medium voltage PMSM drive and its control method," in *IEEE Access*, vol. 11, pp. 92796–92806, 2023.

[3] A. Marzoughi, R. Burgos, D. Boroyevich, and Y. Xue, "Design and comparison of cascaded H-bridge, modular multilevel converter, and 5-L active neutral point clamped topologies for motor drive applications," in *IEEE Transactions on Industry Applications*, vol. 54, no. 2, pp. 1404–1413, Mar.-Apr. 2018.

[4] Y. Zhang, Z. Guo, H. Li, and F. Peng, "A low-cost active reflected wave canceller for MMC motor drive using SiC devices," in *2022 International Power Electronics Conference (IPEC-Himeji 2022- ECCE Asia)*, Himeji, Japan, 2022, pp. 1090–1094.

[5] A. J. Korn, M. Winkelnkemper, and P. Steimer, "Low output frequency operation of the modular multi-level converter," in *2010 IEEE Energy Conversion Congress and Exposition*, Atlanta, GA, USA, 2010, pp. 3993–3997.

[6] J. Yu and C. Xia, "Capacitor voltage fluctuation suppression method based on improved MMC topology for variable-frequency drive application," in *CPSS Transactions on Power Electronics and Applications*, vol. 7, no. 2, pp. 150–159, Jun. 2022.

[7] Y. Zhang, Y. Zhang, and Z. Wang, "Reliability-oriented adaptive switching frequency scheme for modular multilevel converters," in *CPSS Transactions on Power Electronics and Applications*, vol. 9, no. 1, pp. 1–9, Mar. 2024.

[8] S. Jiang and Z. Bai, "Low frequency operation control method for modular multilevel converter based on improved arm current prediction," in *2023 IEEE 6th International Electrical and Energy Conference (CIEEC)*, Hefei, China, 2023, pp. 1346–1351.

[9] S. Du, B. Wu, N. R. Zargari, and Z. Cheng, "A flying-capacitor modular multilevel converter for medium-voltage motor drive," in *IEEE Transactions on Power Electronics*, vol. 32, no. 3, pp. 2081–2089, Mar. 2017.

[10] S. Du, B. Wu, and N. Zargari, "A control strategy for star-channel modular multilevel converter in variable-speed motor drive application," in *IEEE Transactions on Industrial Electronics*, vol. 66, no. 7, pp. 5094–5101, Jul. 2019.

[11] S. Du, B. Wu, and N. R. Zargari, "A delta-channel modular multilevel converter for zero/low-fundamental-frequency operation," in *IEEE Transactions on Industrial Electronics*, vol. 66, no. 3, pp. 2227–2235, Mar. 2019.

[12] R. Aguilar, L. Tarisciotti, and J. Pereda, "Circulating current suppression in DAB assisted low-voltage variable frequency MMC," in *IEEE Transactions on Industry Applications*, vol. 58, no. 5, pp. 6322–6331, Sept.-Oct. 2022.

[13] Zhang, T. Song, Y. Qi, H. Li, S. Hua, and J. Cai, "Research on improved low frequency control strategy of MMC driven permanent magnet synchronous motor," in *2022 China International Conference on Electricity Distribution (CICED)*, Changsha, China, 2022, pp. 971–975.

[14] N. Aarzoo and G. Poddar, "Input current source-based modular multilevel converter for wound field synchronous machine drive with improved low-speed operation," in *IEEE Journal of Emerging and Selected Topics in Industrial Electronics*, vol. 4, no. 1, pp. 419–429, Jan. 2023.

[15] Z. Li, Q. Song, B. Zhao, Z. Yu, R. Zeng, and B. Cui, "Analysis of ride-through capability of unidirectional-current MMC with arm current unidirectionality disrupted," in *IEEE Transactions on Power Electronics*, vol. 39, no. 8, pp. 9257–9267, Aug. 2024.

[16] J. Han and C. Liu, "Quasi proportional resonant controller based MMC grid side harmonic suppression research," in *2022 IEEE International Conference on Power Systems and Electrical Technology (PSET)*, Aalborg, Denmark, 2022, pp. 240–245.

[17] W. Chao, J. Huang, C. Deng, and L. Dai, "Fuzzy adaptive PI circulating current suppressing control for MMC-HVDC," in *2023 IEEE 6th Information Technology,Networking,Electronic and Automation Control Conference (ITNEC)*, Chongqing, China, 2023, pp. 1163–1167.

[18] H. Wang, P. Huang, Y. Chen, Z. Lin, and R. Huang, "Impedance coupling suppression mechanism of high-voltage direct-current transmission system with large-scale renewable energy," in *2023 10th International Forum on Electrical Engineering and Automation (IFEEA)*, Nanjing, China, 2023, pp. 738–743.

[19] S. Jakkula, N. P. Rao, and A. Shukla, "A novel circulating current suppression control utilizing negative insertion in MMC," in *2024 IEEE Applied Power Electronics Conference and Exposition (APEC)*, Long Beach, CA, USA, 2024, pp. 238–243.

[20] Q. Wang, H. Ye, and G. Zhang, "Analysis of the circulating current characteristics of MMC in DQ frame," in *2017 IEEE Conference on Energy Internet and Energy System Integration (EI2)*, Beijing, China, 2017, pp. 1–6.

[21] Y. Wang, C. Zhao, and R. Iravani, "Small signal stability investigation of the MMC-HVDC grid," in *IEEE Transactions on Power Delivery*, vol. 37, no. 5, pp. 4448–4459, Oct. 2022.

[22] R. Mishra and V. Agarwal, "Modified series chain link MMC for offshore wind farms with boosted AC voltage: Frequency-domain modeling and submodule capacitor voltage ripple optimization," in *IEEE Transactions on Industrial Electronics*, vol. 70, no. 9, pp. 8676–8687, Sept. 2023.

[23] J. Xu, J. Wang, Y. Yang, J. Wang, and G. Li, "Optimal suppression strategy for capacitor voltage ripples of hybrid MMCs under unbalanced grid voltages," in *IEEE Transactions on Power Delivery*, vol. 38, no. 1, pp. 244–254, Feb. 2023.

[24] X. Chen and J. Zhang, "MMC circulation suppression optimization strategy based on quasi-PIλR controller," in *2023 IEEE International Conference on Advanced Power System Automation and Protection (APAP)*, Xuchang, China, 2023, pp. 167–172.

Jianfei Zhao received the B.S. and M.S. degrees in Mechatronic Engineering from the Xi'an Jiaotong University, Xi'an, China, in 2000 and 2003, respectively. He received the Ph.D. degree in Electrical Engineering from Shanghai Jiao Tong University, Shanghai, China, in 2012. From 2003 to 2006, he worked as a R&D Engineer and Project Manager in R&D Center of Myway-labs Co.,Ltd in Japan. Now, he is working as an Associate Professor with the Mechatronic Engineering and Automation School, Shanghai University. He is the author of more than 50 academic papers. His research interests include power electronics and electronic vehicles. Dr. Zhao was a recipient of the Science and Technology Progress Award of the Ministry of Education of China in 2009 and 2012, the Science and Technology Progress Award of Shanghai City in 2019, the Science and Technology Progress Award of China Electrotechnical Society in 2009 and 2010.

Sucheng Huang received the B.S. degree in Electrical Engineering and Automation from Shanghai University, Shanghai, China, in 2024 and now he is pursuing the M.S. degree in Electrical Engineering at the same university. His research interest mainly involves in the drive control of new energy electric vehicles.

Yuanyuan Xing received the B.S. degree in Electrical Engineering and Automation from Shanghai University, Shanghai, China, in 2023, where she is currently pursuing the M.S. degree in electrical engineering. Her research interests include electric vehicle drive control and new energy generation.